Investigation of Ne IX and Ne X line emission from dense plasma using Ross-filter systems

E. Kroupp, A. Starobinets, E. Klodzh, Yu. V. Ralchenko, and Y. Maron
Faculty of Physics, Weizmann Institute of Science, Rehovot 76100, Israel

I. N. Bogatu
FARTECH Inc., 10350 Science Center Dr., Building 14, Suite 150, San Diego, California 92121

A. Fisher
Technion–Israeli Institute of Technology, Haifa, Israel

(Received 20 May 2002; accepted 6 August 2002)

We report on the application of well-balanced Ross-filter systems for the diagnostics of x-ray emission from a *Z*-pinch plasma. The composition and thicknesses of the filter layers were so selected to yield the intensities of neon H- and He-like emission lines separately with relatively good accuracy. The systems provide convenient absolute and time-dependent measurements of the emission intensities, and they are particularly useful for relatively low source-light intensities. The applicability of the systems is examined with the aid of time-dependent modeling of the stagnating plasma, using collisional-radiative and radiation transport calculations. The data and modeling are used to yield information on time evolution of the plasma density and temperature at stagnation. [DOI: 10.1063/1.1512316]

I. INTRODUCTION

X-ray emission is widely used in the diagnostics of hot plasmas, both in laboratory and in astrophysics. In this article, we report on the investigation of a *Z*-pinch plasma stagnating on axis by the use of Ross (or balanced) filters[1,2] for x-ray filtration. Coupling these filters to semiconductor detectors that are sufficiently fast provides rather convenient absolute emission-intensity measurements that are resolved in spectrum, space, and time. Due to their high light collection efficiency relative to crystal spectroscopy systems, such devices can be particularly useful for relatively low light intensities.

A basic Ross-filter system consists of two filtration channels that view the same plasma volume, each including an x-ray absorbing layer followed by an identical x-ray detector. The layers of the two channels are made of elements (or compounds) of similar atomic numbers *Z*. The thicknesses of the layers in the two channels are adjusted to achieve almost equal transmission curves for the two channels over the entire photon energy range, except within the narrow spectral region between the layer absorption edges (usually L_{III} or K edges). The subtraction of the transmission curves of the two channels thus gives an almost zero value in most of the photon energies except for the spectral region between these absorption edges, which constitutes the Ross-filter passband. The subtraction of the two channel-detector signals thus yields the total incident x-ray power within the Ross-filter passband.

An essential requirement for an efficient Ross filter is a satisfactory balancing of the two channels outside the passband, in order to minimize the signal due to continuum and line radiation outside the band. In this study, using detailed iterative calculations of the photon absorption in the layers, based on tables published by Henke *et al.*,[3] the layer compositions and thicknesses were so selected to provide almost perfect balancing outside the passband and the maximum transmission inside the band.[4] Another advantage of the Ross filters here employed is the narrow passband achieved by the use of elements with successive *Z* numbers, due to the spectral proximity of their absorption edges. This allows for both reducing the continuum radiation and the number of lines within the passband, which improves the reliability of the interpretation of the Ross-filter signals.

The Ross-filter systems presented here are designed for the investigation of He-like and H-like neon. Lines of such charge states are used extensively in the studies of imploding plasmas.[5] The Ross filters were so designed to allow the Ne IX and Ne X line radiation to be determined separately. Measurements for a *Z*-pinch plasma column at stagnation and the data analysis are presented below.

II. EXPERIMENTAL SETUP

The Ross-filter systems used in the present experiment utilize four L_{III} edges. The filters are micron and submicron layers of Ni, Cu, Zn, or Ga_2O_3, which were coated on a soft x-ray transparent support. The layers were produced by single, double, or triple coatings,[6] where each pair of the four layers provides a spectral passband.

The passbands used in our experiment include a band between 852.7 eV (Ni L_{III} edge) and 932.5 eV (Cu L_{III} edge), here denoted by Filter I. The transmission curves for each channel and the resulting transmission curve of the Ross filter are shown in Fig. 1. The filter transmits the neon He_α line, the intercombination line, and the He_α satellites. The other band, Filter II, is between 932.5 and 1021.8 eV (Zn L_{III} edge), transmitting the Ly_α and most of its satellites, as shown in Fig. 2. The Zn L_{III} edge lies between the 1/2-1/2 (1021.5 eV) and 1/2-3/2 (1021.95 eV) fine-structure compo-

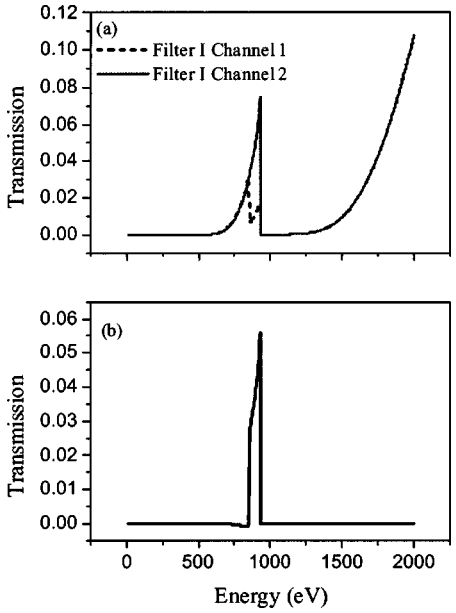

FIG. 1. (a) Transmission curves of the two channels of Filter I. Channel 1 includes: 0.15 μm of Ni, 0.96 μm of Cu, and 0.1 μm of parylene–N. Here, the Cu layer was added to improve the matching of the two channels. Channel 2 includes: 1.1 μm of Cu and 0.1μm of parylene–N. The transmission curves shown also account for the 7.5-μm-thick Be foil used for all channels, (b) The transmission curve of Ross-filter I, obtained by the subtraction of Channel 1 from Channel 2.

nents of the neon Ly_α, thus only transmitting part of the Ly_α, which is accounted for in the data analysis given below. The third band, Filter III, is between 1021.8 and 1116.7 eV (Ga L_{III} edge), thus transmitting the Ly_α part that is not transmitted by Filter II, besides He_β, the He_β intercombination

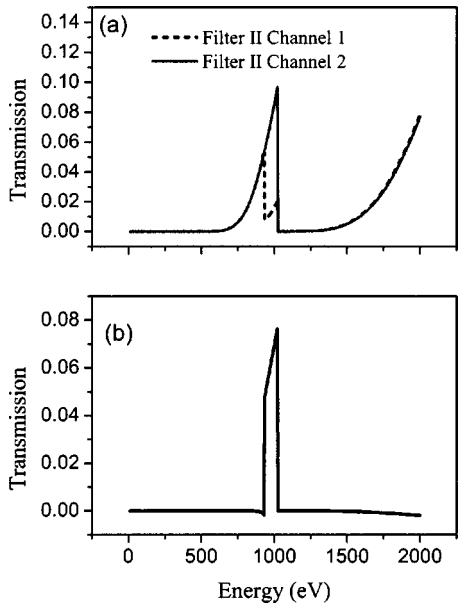

FIG. 2. (a) Transmission curves of the two channels of Filter II. Channel 1 includes: 0.2 μm of Cu, 1.2 μm of Zn, and 0.1 μm of parylene–N. The Zn layer was added to improve the matching of the two channels. Channel 2 includes: 1.44 μm of Zn and 0.1μm of parylene–N. The transmission curves shown account for the 7.5-μm-thick Be foil used for all channels, (b) The transmission curve of Ross-filter II, obtained by the subtraction of Channel 1 from Channel 2.

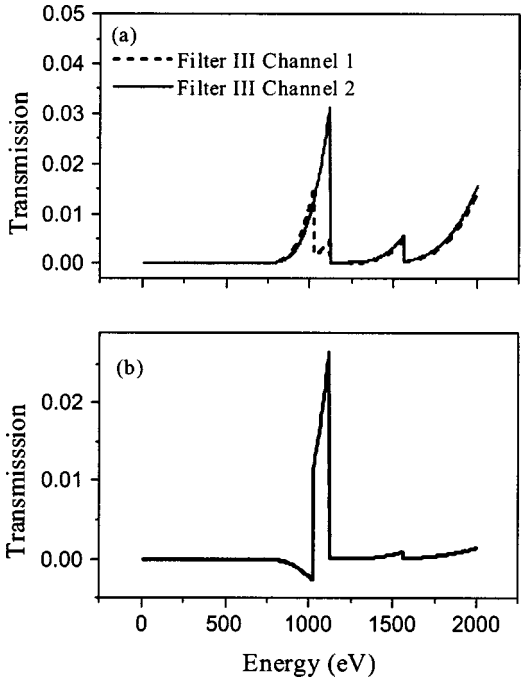

FIG. 3. (a) Transmission curves of the two channels of Filter III. Channel 1 includes: 0.35 μm of Zn, 1.6 μm of Ga_2O_3, 0.1 μm of parylene–N, and 2.5-μm of Al. Here, the Ga_2O_3 layer was added to improve the matching of the two channels. Channel 2 includes: 2 μm of Ga_2O_3, 0.1 μm of parylene–N, and 2.5 μm of Al. The transmission curves shown also account for the 7.5-μm-thick Be foil used for all channels, (b) The transmission curve of Ross-filter III, obtained by the subtraction of Channel 1 from Channel 2.

line, and the He_β satellites, as shown in Fig. 3. The radiation through all filters first passes through a 7.5- μm-thick Be foil.

For the signal detection, we used Quantrad x-ray diodes with a 3-mm^2 sensitive area, and with a 0.7-μm-thick Si entrance window followed by a 35-μm-thick Si layer, which allows for sufficiently fast response (the sensitivity curves of the diodes were accounted for in the data analysis given below).

The experiment was performed using a 1.2-μs, 300-kA gas- puff *Z*-pinch system. Using neon as the working gas, a plasma column 14 mm in length and about 1 mm in diameter is formed at stagnation on axis, with its temperature being in the range of hundreds of electronvolts, leading to a 20–30-ns duration x-ray emission dominated by Ne IX and Ne X lines.

The Ross-filter systems were placed 88 cm from the pinch axis viewing the plasma column from the side, yielding the time-resolved intensities in the three spectral windows given above simultaneously. The axial spatial resolution was set by a collimator to be 1.6 mm and the temporal resolution was 3 ns.

III. MEASUREMENTS AND DATA ANALYSIS

In examining the Ross-filter system, it is primarily required to verify that the signals of the two channels, when operated using an identical filter, yield by their subtraction a zero signal. This examination is of special importance for fast-rising signals that require the use of identical fast elec-

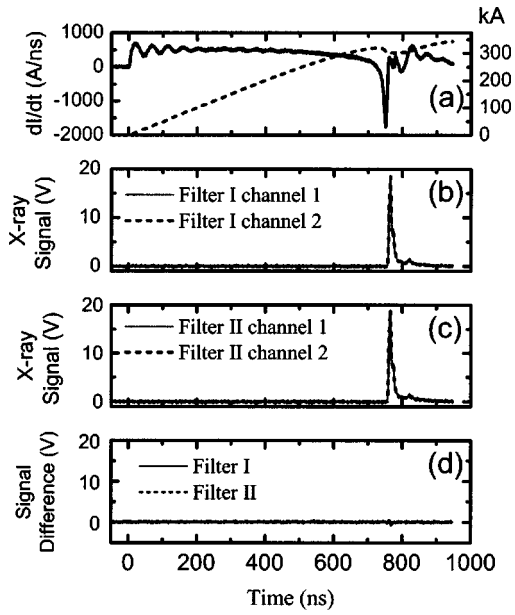

FIG. 4. Examination of the channel balance. (a) Traces of dI/dt (solid line) obtained from a B-dot probe and the current I (dashed line); (b) The signals of the two channels of Filter I measured through a 15-μm-thick Be and 1.1-μm-thick Cu foils; (c) The same as (b) for Filter II, (d) The signals of Filters I and II resulting from the subtraction of the two channels in (b) and (c), respectively.

tronics and cable lengths. For this examination, we used a 15-μm-thick Be filter covered by a 1.1-μm-thick Cu foil for all four detectors (the Cu foil was required for avoiding the signal saturation). The difference of the signals of the various pair channels allowed for examining the balancing of the channels, together with assessing the signal noise level, as shown in Fig. 4. Such measurements showed that the various channels were balanced to within 3%. Also, the absence of any signal prior to the plasma stagnation on axis demonstrates that no radiation other than the x-ray radiation at stagnation reaches the detectors.

In Fig. 5 we present examples of signals measured using Filters I and II (in the present article only measurements with these two filters are presented). It is seen that the signal of Filter I starts about 3–4 ns prior to and lasts ~20 ns after the signal of Filter II, indicating the longer presence of the He-like relative to the H-like ions. In the experiment, the measured total peak x-ray emission powers, from the pinch axial portion observed, ranged between 80 and 130 and 30 and 40 MW within the passbands of Filters I and II, respectively.

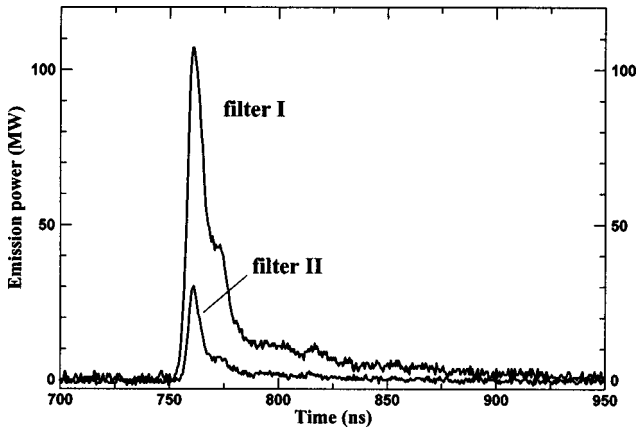

FIG. 5. Total radiation power measured with Filters I and II.

In interpreting the signals obtained from the Ross filters, three factors have to be accounted for: The spectral lines that lie within the filter passband; the continuum radiation within the band; and the signal resulting from the x-ray radiation outside the passband, allowed for by the imperfect balancing of the two channels. The effect of each of these factors evidently depends on the specific parameters of the plasma studied.

The assessment of the relative importance of these factors requires modeling the plasma at stagnation. Radiation from plasmas in *Z* pinches has been modeled, for example in, Ref. 7, where the plasma was assumed to be in collisional-radiative equilibrium. Such an assumption is expected to be satisfactory for sufficiently dense plasmas or for plasmas with properties that vary relatively slowly in time. Our calculations demonstrate that these requirements are not fulfilled for the conditions of the stagnating plasma in the present experiment. We thus used a simulation of the plasma emission that accounts for the time dependence of the plasma properties and assumes no collisional-radiative equilibrium. The simulation was carried out using the time-dependent collisional-radiative model described in detail in Ref. 8. Briefly, the time-dependent rate equations are solved for all ions of neon assuming the plasma is a uniform column with a prescribed time-dependent electron temperature $T_e(t)$. The model also assumes a constant total mass M within the plasma column and a time-dependent plasma outer radius $R(t)$, which together fix the ion density $n_i(t)$, where the electron density $n_e(t)$ is calculated from the plasma neutrality condition.

The following atomic processes were accounted for in the rate equations: electron-impact excitation, deexcitation, and ionization; three-body, radiative and dielectronic recombination; spontaneous radiative decays; autoionization, and dielectronic capture. The elementary characteristics of the kinetic processes, which are the process cross-sections and transition probabilities, were mainly calculated with the ATOM code[9] for collisions and the RCN/RCN2/RCG Hartree-Fock code[10] for radiative and autoionization probabilities.

Calculations were performed for various temporal functions of the electron temperature and of the plasma outer radii in the range relevant to our *Z*-pinch plasma. The values of the mass M, constant for each calculation, were taken between 1 and 3 μg/cm, consistent with the known initial mass in the gas puff, $\cong 18$ μg/cm, and the knowledge that a small fraction of the initial gas participates in the final plasma compression phase.[11] The rest of the mass in the gas puff was ignored in the present modeling. The values used for the minimal radius of the plasma column (peak compression) were between 0.3 and 1 mm, consistent with the x-ray pinhole pictures of our *Z*-pinch plasma.[12]

Since the x-ray emission within the filter bands originates primarily from the highest-charge ions, the collisional-radiative modeling was done with the emphasis on a detailed description of the Li-, He-, and H-like ions of neon. The

number of states (mostly atomic terms) in these ions, including the autoionizing levels, was about 40, 45, and 15, respectively. Since the $n=2$ to $n=1$ transitions provide most of the emission within the filter passbands, the $1s2p\ ^3$P term in Ne IX and the $n=2$ state in Ne X were split into the fine-structure components ($2s_{1/2}$, $2p_{1/2}$, and $2p_{3/2}$ for the latter), to achieve the most accurate simulation of the *K*-shell emission. This is especially important for the Ly_α emission since in our experiment, as stated above, its 1/2 and 3/2 components were recorded by different filters. The emission of the satellites to the He_α and Ly_α resonance lines, due to the dielectronic and inner-shell excitation processes, has also been modeled in detail, with proper account of all coupling channels between them and other levels.

The optical thickness for the line transitions in the stagnating plasma was calculated in the present simulations, assuming the line shapes are Doppler dominated and the ion temperature is equal to $T_e(t)$. These assumptions yield optical depth values of 15–30 for the H- and He-like-ion resonance lines emitted radially out of our plasma column (it is estimated that in reality, the optical thickness values can be up to three times lower due to possible larger contribution of the Doppler broadening to the linewidths). The effect of the optical thickness on the level populations was taken into account in the escape factor approximation. Such calculated populations were then used to solve the radiation transfer equation and to synthesize the plasma emission spectrum within the filter bands.

IV. RESULTS AND DISCUSSIONS

Using this modeling, we calculated the intensities of lines within the passbands of all filters, including the intercombination and satellite lines. The continuum radiation (free–free and free-bound) was also calculated for various plasma densities and temperatures within the relevant range of our plasma parameters, and found to contribute about 2% to the total light intensities within the passbands of the filters used. We thus used the modeling described above to fit the intensity of the line radiation within the passbands of all filters.

A satisfactory fit for the data obtained using this modeling is shown in Fig. 6(a), together with the experimental signals of Filters I and II (given in Fig. 5), zoomed at the time of peak emission. Based on this rather satisfactory fit for the two-filter data, it is seen that within the assumptions of this modeling, these data allowed for obtaining information on the peak electron temperature, about 280 eV, and the electron density, about 6×10^{19} cm^{-3} (i.e., an ionic density of about 6×10^{18}cm^{-3}), in the presently studied *Z*-pinch column. An apparently less satisfactory agreement of the modeling results with the Filter I data may result from plasma nonuniformity, which is not accounted for in our modeling. Note that the measurement of the absolute Ne IX and Ne X line intensities was essential in obtaining bounds on the total plasma mass *M* (and the ion density) in the plasma column, which in turn affects the opacity effects in the plasma and the ionization rates (through the value of the electron density).

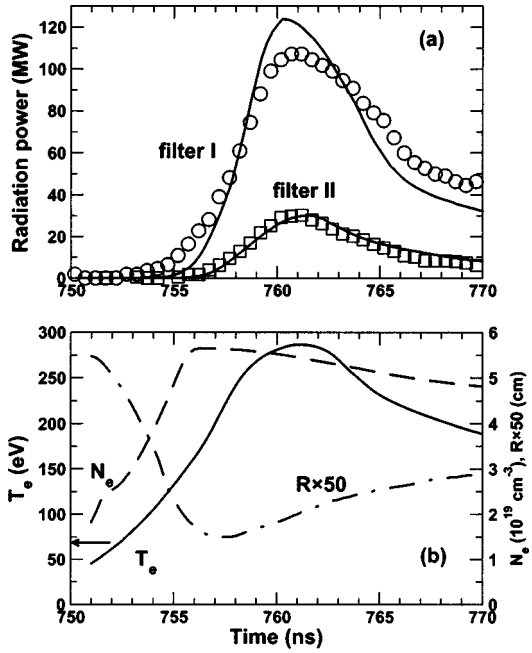

FIG. 6. (a) Total radiation power within the pass bands of Filters I and II at the time of the emission peaks. Experimental data are shown by symbols and the simulation results by solid curves, (b) The electron temperature $T_e(t)$ and outer plasma radius $R(t)$ used in the simulations given in (a). Here, the mass density was assumed to be 1.5 μg/cm, and the resulting electron density $n_e(t)$ is given in the figure.

It is noteworthy that found in our modeling is that most of the satellite lines within the filter passband result from dielectronic recombination of H-like and He-like ions (rather than inner-shell excitations of He-like and Li-like ions, respectively). Thus, the line intensities recorded by Filters I and II are proportional to the total abundances of the He- and H-like ions, respectively. This allows direct information on the densities of Ne IX and Ne X to be obtained from the signals of the Ross filters here used. The densities of Ne VIII to Ne XI predicted by the modeling described in Fig. 6 are shown in Fig. 7.

As stated above, there is a need to estimate the measurement error resulting from the detection of the radiation outside the passbands, due to the incomplete balancing of the

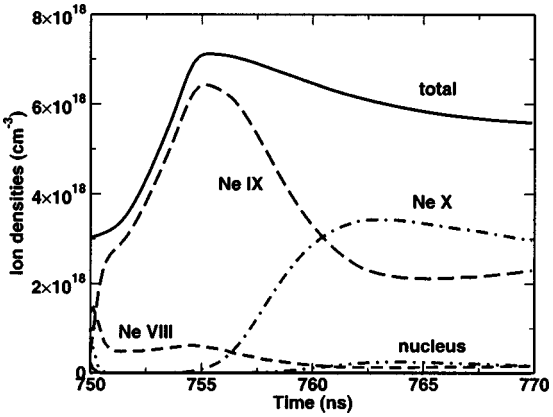

FIG. 7. Absolute densities of the high-charge states of neon (Ne VIII to Ne XI) and the total ion density for the plasma parameters of Fig. 6.

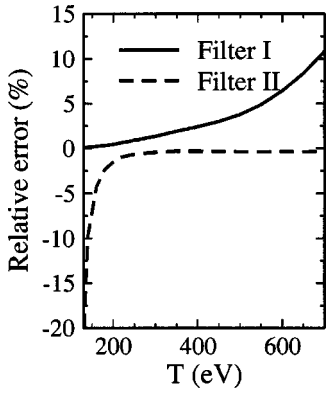

FIG. 8. The relative error (in percent) in measuring the radiation within the pass bands of Filters I and II as a function of the electron temperature. Here, steady-state collisional-radiative calculations were made and the electron density was assumed to be 1×10^{20} cm^{-3}.

channels. To this end, we used the modeling described above to calculate the spectra over the entire energy range of the photons detectable by the *p-i-n* detectors and used the transmission curves of the two channels to compute the signal resulting from the radiation outside the Ross-filter passband. Evidently, the relative error depends on the plasma parameters. An example of an error calculation is given in Fig. 8 for plasma parameters typical to our experiment. It is seen that the relative error in Filter II may rise to 20%, for temperatures below 150 eV for which the Ne X abundance is low, because of the relatively small contribution of the Ne X emission within the bandpass of the filter. The negative sign of the error is due to a negative transmission of Filter II around the emission energies of Ne IX, which is the dominating charge state for such a low temperature (the error is much smaller for higher T_e, where the abundance of Ne X is high). The positive sign of the error in Filter I is due to the positive transmission of the tail of this filter at high photon energies, resulting from the continuum radiation contribution at high temperatures. Using such calculations, it was found that for $n_e\sim10^{19}-10^{20}$ cm^{-3} and $T_e=130-700$ eV the error due to the incomplete channel balancing for our Ross filters ranges between 3% and 20% (usually smaller than 20%).

In summary, it was demonstrated that Ross-filter systems can serve as a convenient tool for obtaining rather accurate time-dependent and absolute measurements of x-ray emission from hot plasmas. Measurements of Ne IX and Ne X line radiation using such systems, together with time-dependent collisional-radiative and radiation-transport modeling, allowed for studying the properties of the stagnating plasma in a gas-puff *Z*-pinch experiment operating with a current at the 300-kA level. Further information on such a plasma can be obtained by combining the Ross-filter measurements with data obtained from additional spectroscopic x-ray diagnostics.

ACKNOWLEDGMENTS

The authors are indebted to V. I. Fisher for valuable discussions on the data analysis and the radiation transport. The skilled technical support of P. Meiri is highly acknowledged. This work is supported in part by the German-Israeli Foundation, the Israeli Science Foundation Grant No. 6858, and Sandia National Laboratories (USA).

[1] P. A. Ross, Phys. Rev. **28**, 425 (1926).
[2] P. A. Ross, J. Opt. Soc. Am. **16**, 433 (1928).
[3] B. L. Henke, E. M. Gullikson, and J. C. Davis, Ann. Rheum. Dis. **54**, 181 (1993).
[4] I. N. Bogatu, L. Gregorian, E. Klodzh, E. Kroupp, Y. Maron, and Yu. V. Ralchenko, *Proceedings of the 12th International Conference on High-Power Particle Beams (BEAMS-98)* (Haifa, Israel, 1998).
[5] D. Mosher, S. J. Stephanakis, J. P. Apruzese, D. C. Black, J. R. Boller, R. J. Comisso, M. S. Myers, G. G. Peterson, B. V. Weber, and F. C. Joung, in *Proceedings of the 4th International Conference on Dense Z-Pinches*, edited by N. R. Pereira, J. Davis, and P. E. Pulsifer (Vancouver, Canada, 1997).
[6] Lebow Co., Goleta CA 93117.
[7] J. P. Apruzese, K. G. Whitney, J. Davis, and P. C. Kepple, J. Quant. Spectrosc. Radiat. Transfer. **57**, 44 (2001).
[8] Yu. V. Ralchenko and Y. Maron, J. Quant. Spectrosc. Radiat. Transfer. **71**, 609 (2001).
[9] V. P. Shevelko and L. A. Vainshtein, *Atomic Physics for Hot Plasmas* (IOP Publishing, Bristol, 1993).
[10] R. D. Cowan, *Theory of Atomic Structure and Spectra* (University of California, Berkeley, 1981).
[11] J. W. Thornhill, K. G. Whitney, J. Davis, and J. P. Apruzese, J. Appl. Phys. **80**, 710 (1996).
[12] E. Kroupp, Ph.D. Thesis, Weizmann Institute of Science, Rehovot, Israel (2002).